X-ray specular reflectivity study of a critical binary fluid mixture

L. W. Marschand,[1] M. Brown,[2] L. B. Lurio,[1] B. M. Law,[2] S. Uran,[2] I. Kuzmenko,[3] and T. Gog[3]
[1]*Department of Physics, Northern Illinois University, DeKalb, Illinois 60115, USA*
[2]*Department of Physics, Kansas State University, Manhattan, Kansas 66506, USA*
[3]*Advanced Photon Source, Argonne National Laboratory, Argonne, Illinois 60439, USA*
(Received 19 November 2004; revised manuscript received 27 April 2005; published 28 July 2005)

We have used direct inversion of x-ray reflectivity data to extract the liquid-vapor interface composition profile and the related critical scaling function of a binary mixture of dodecane and tetrabromoethane. The mixture was in the one-phase region above its critical point. The results indicate the formation of a monolayer of the lower surface tension component followed by an abrupt change to a mixed composition which gradually relaxes to the bulk composition deep within the fluid.

DOI: 10.1103/PhysRevE.72.011509 PACS number(s): 64.75.+g, 64.60.Fr, 68.03.−g

I. INTRODUCTION

At the liquid-vapor interface of a binary fluid mixture, the component with the lowest surface tension will segregate to the surface even above the temperatures where the two fluids are mixed in the bulk. With increasing depth, z, into the fluid, the composition returns to its bulk value. Near the critical point, the length scale over which the composition returns to its equilibrium value will be determined by the bulk-fluid correlation length $\xi=\xi_0 t^{-\nu}$ with ξ_0 a correlation length amplitude, $t=(T-T_c)/T_c$, and ν a critical exponent. For systems in the 3D Ising universality class it is expected that $\nu \approx 0.632$.

Based on the predictions of Fisher and de Gennes [1], very close to the critical point, and in the limit of a sufficiently strong and short range surface field, h_1, the profile should have a universal scaling form given by

$$m(x) = Mt^{\beta}P(x). \tag{1}$$

Here the order parameter, m is related to the volume fraction of the surface segregating component via $m=\Phi(z)-\Phi(\infty)$ and Mt^{β} describes the shape of the coexistence curve for the specific binary fluid mixture. The depth into the fluid is given as a function of dimensionless coordinates $x=(z+ze)/\xi$ *where* z_e *is a system dependent offset value. The critical exponent* β *is expected to have the value of about 0.328.*

Based on simple scaling arguments, the limiting forms of the universal function, P, for small and large x are expected to be

$$P(x) \to P_0 x^{-\beta/\nu} \quad \text{for} \quad x \to 0,$$

$$P(x) \to P_\infty e^{-x} \quad \text{for} \quad x \to \infty, \tag{2}$$

where the small and large x behavior originate from, respectively, Fisher and de Gennes [1] and Liu and Fisher [2]. The theoretical predictions of Fisher and de Gennes have been subsequently refined by Monte Carlo [3], renormalization group [4] and an interpolation scheme [5], which gave rise to values of 0.866, 0.717 and 0.94±0.05, respectively, for P_0 and 1.5 and 1.621, respectively for P_∞ (the interpolation scheme did not provide a prediction for P_∞). There have also been a number of experimental tests. Light reflection measurements probe integrals over the critical adsorption profile, and are mainly sensitive to the temperature dependence of scaling variables. Schlossman *et al.* used optical reflectivity to confirm the asymptotic behavior predicted in Eq. (2) [6]. A summary of ellipsometry studies, which measures the optical reflectance at the Brewster angle, has been published by Carpenter *et al.* [7]. These authors find they can describe a wide range of results using a model denoted $P1$, which uses asymptotic limits for the scaling function up to second order in an expansion in the large x and small x regions where x is the dimensionless parameter defined above [8]. These limits are matched at a crossover point, x_0 (the only freely adjustable parameter) up to their first derivative in x. They were able to fit ellipsometry data from five different critical binary fluids using values of $P_0=0.788$, $P_\infty=0.963$, and $x_0=1.15$ [7,9]. Direct tests of the shape of the profile have been made via neutron scattering measurements [10–12]. Howse *et al.* studied a system of 2-butoxyethanol+deuterium oxide. The neutron scattering data were well described by a model using a power law profile for small x with an exponent of 0.52±0.02. This is within errors of the predicted value of $\beta/\nu=0.516$. They found $P_0=0.11$; significantly smaller than the expected value from Monte Carlo calculations of 0.866 [3]. Zhao *et al.* studied methanol+deuterated cyclohexane. Their neutron measurements could be fit with a scaling form proposed by Liu and Fisher:

$$P(x) = P_0[(1+cx)/x]^{\beta/\nu}\exp(-x). \tag{3}$$

The parameters β/ν and P_0 were coupled in the fits. If they fixed $P_0=1$ then $\beta/\nu=0.50\pm0.05$, while for β/ν fixed to its theoretical value, $P_0=0.34$. Jestin *et al.* looked at *n*-hexane+perfluorohexane and methanol+cyclohexane with either of the two components deuterated. They obtained good neutron reflectivity fits with the Liu-Fisher form. The methanol+cyclohexane mixtures gave values of P_0 close to the predicted 0.866, but β/ν were 5 to 10% smaller than theory. For *n*-hexane+perfluorohexane they obtained $P_0=1.78$ which is much larger than theory. They hypothesize that this large value of P_0 may indicate a different profile shape for the case of a large surface tension difference between the components.

All of the neutron scattering measurements, to date, have been limited to small wave-vector transfer, defined by $Q = 4\pi \sin(\theta)/\lambda$, with θ the incident angle. In the present measurement we have carried out an x-ray specular reflectivity measurement with high angular resolution, and out to large $Q_{\max} = 2.3\ \mathrm{nm}^{-1}$. This provides sensitivity to features at the molecular length scale such as the formation of a surface monolayer.

In the Born approximation, the intensity of x-ray reflection vs angle can be related to the absolute magnitude of the Fourier transform of the scattering length density.

$$R(Q)/R_F(Q) = \left| \frac{1}{\rho(\infty)} \int_{-\infty}^{\infty} e^{iQz} \frac{d\rho(z)}{dz} dz \right|^2. \qquad (4)$$

Here ρ is the x-ray scattering length density, $R(Q)$ is the measured reflectivity, and $R_F(Q)$ is the ideal Fresnel reflectivity for a perfectly sharp interface.

When multiple scattering cannot be ignored, the reflectivity can be approximated by the Parratt [13] method, in which Maxwell's equations are solved for a system of uniform density slabs that approximate the profile. In neither case can the x-ray scattering data be directly inverted, without further assumptions, since the phase of the reverse Fourier transform is not available. Techniques have been developed, however, that allow the phase to be recovered through the imposition of physical constraints on the possible profiles. These have been recently reviewed by Tolan [14]. We have applied the technique outlined by Sanyal *et al.* [15] to the present data.

II. REFLECTIVITY EXPERIMENT

The sample cell was a Pyrex tray inside a two-staged oven [16]. It was horizontally mounted and fitted with 25 μm thick Kapton windows. The temperature could be held uniform over the chamber to ±1 mK. The sample was a mixture of *n*-dodecane (Fluka 98+% purity) and 1,1,2,2-tetrabromoethane (Aldrich 99+% purity). The chemicals were used as received from the supplier. This mixture yields excellent x-ray contrast, and has previously been studied via ellipsometry [9]. Both components are nonpolar which excludes surface orientational ordering effects [17]. This mixture was prepared to within 1% of its critical composition (45% by volume of dodecane). The sample environment was saturated with the equilibrium vapor of the mixture. In order to minimize vibration, the sample was a thin layer ($<$1.5 mm) of fluid on top of a flat rectangular 19 mm by 45 mm glass slide. The sample was surrounded by a 7 mm deep trough filled with the mixture, but the mixture did not contact the windows, thus avoiding problems associated with a meniscus. Due to poor convective mixing in the thin layer, it was necessary to maintain the sample always above its critical temperature of $T_c = 37.5\,^{\circ}\mathrm{C}$, since, should phase separation occur, the mixture could not be remixed *in situ*. The accumulation of x-ray damage to the sample was prevented by topping the sample cell with fresh mixture after every change in temperature. Reflectivity data were taken from $+1\,^{\circ}\mathrm{C}$ to $+30\,^{\circ}\mathrm{C}$ above T_c. Between measurements the cell was allowed to equilibrate for 2 to 4 h until no gradients larger than 1 mK/cm remained. Measurements were performed at CMC-CAT at the Advanced Photon Source. The measured x-ray reflectivity, normalized to the Fresnel reflectivity $R_F(Q)$ for the bulk mixture, is displayed vs Q, in Fig. 1. Just above the critical angle ($Q_c = 0.277\ \mathrm{nm}^{-1}$) the reflectivity goes below the Fresnel reflectivity. The Q range of the falloff broadens with increasing temperature. There is also a peak in the scattering between 1 and 2 nm^{-1}.

The reflectivity was compared to the $P1$ model of Carpenter *et al.* by converting their profile to an electron scattering length profile. This was divided into $\sim$1000 slabs and the reflectivity was calculated using the Parratt method. This method is discussed in detail by Tolan [14] and Daillant [18]. The model reflectivity did not agree with the measured data. Varying the parameters of the model, (P_0, P_∞, and x_0) did not improve the fits enough to provide a good match to the data because of the peak at $\sim 1\ \mathrm{nm}^{-1}$.

In order to obtain a composition profile which could describe the data, the x-ray data was inverted using the phase guessing algorithm described by Sanyal *et al.* [15]. The basis of this method is to calculate an estimate of the density profile from a reverse transform of the measured scattering. A guess is made for the phase of the transform based on a model profile. For the present study, the initial phase guess was obtained from the $P1$ model, using the Parratt method described above to calculate the model reflectivity. This model profile is iterated, until the reverse transform is consistent with the initial model. Note that while a reverse Fourier transform is used to calculate the phases in this method, the actual reflectivity is calculated from the density profile using the Parratt formalism, which fully accounts for multiple scattering.

Explicitly, the $(m+1)$ iteration of the density profile was calculated via

$$\frac{d\rho_{m+1}(z)}{dz} = \frac{1}{2\pi} \int \int_{-\infty}^{\infty} \exp[iQ(z-z')] \times \sqrt{\frac{R_{ex}(Q)}{R_m(Q)}} \left(\frac{d\rho_m(z')}{dz'} \right) dz'\, dQ. \qquad (5)$$

The subscripts m and ex indicate the model and experimental parameters, respectively. The resulting $d\rho(z)/dz$ was modified by subjecting it to physical constraints and the procedure was iterated. We imposed two physical constraints on the fitting inversion process. The first consisted of the imposition that the liquid-vapor interface be reasonably sharp, which was accomplished by setting the profile to zero for $z < -2$ nm. The second constraint was imposing a monotonically increasing tetrabromoethane concentration from the surface to the bulk, by taking $\rho(z) \rightarrow |\rho(z)|$. This second constraint is physically reasonable, since the dodecane has the lower surface tension and would be expected to dominate the liquid-vapor interface, and since all present theoretical predictions for the profile are monotonic. It should be recognized that this inversion procedure might exclude other possible inversions of the scattering data, which would involve oscillations in the dodecane concentration near the surface. In order to avoid truncation artifacts the reflectivity curve

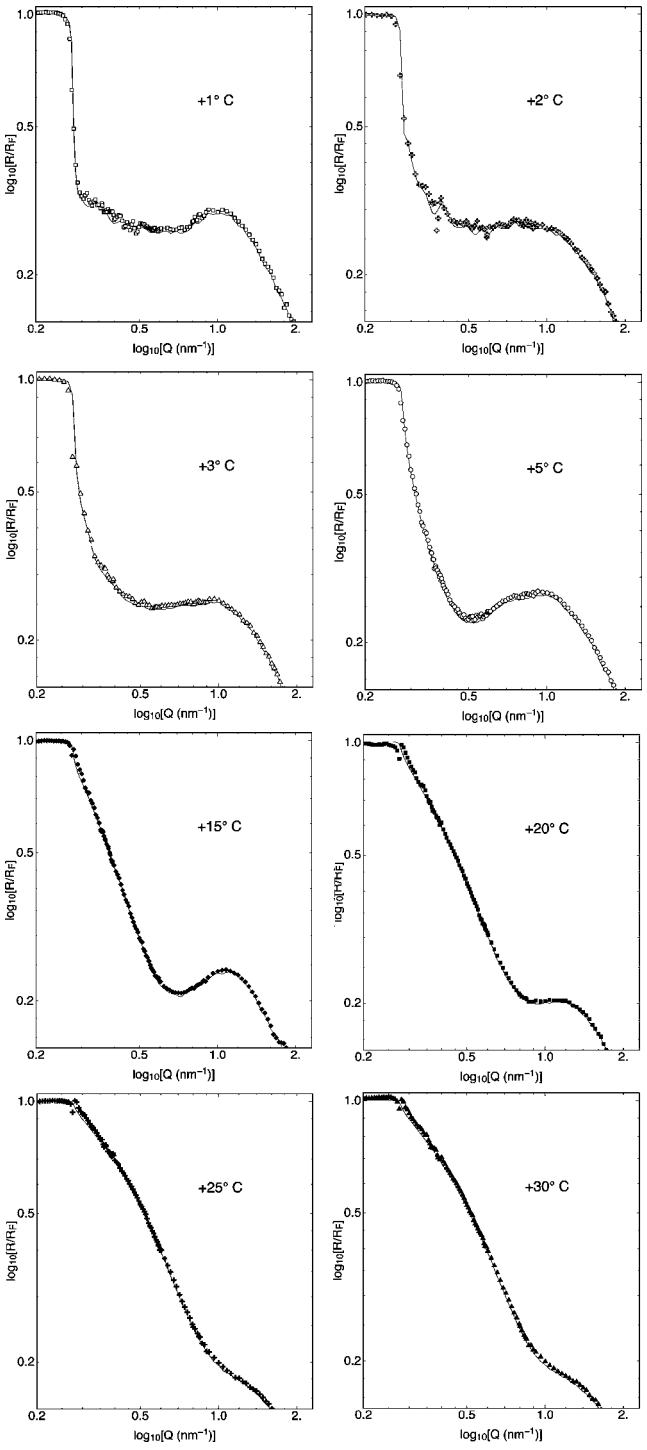

FIG. 1. X-ray reflectivity R/R_F from a mixture of dodecane and tetrabromoethane vs Q. The data are normalized by the Fresnel reflectivity for the bulk. The temperatures, relative to T_c, are +1 °C, +2 °C, +3 °C, +5 °C, +15 °C, +20 °C, +25 °C, and +30 °C. The solid lines are the fits described in the text.

was extrapolated to larger Q by matching a Gaussian tail to the data. Finally, a small ($\sim 10^{-7}$ rads) angular offset was applied to the data so that the critical angle of the simulated density profile would be equal to that of the critical mixture. Such an offset is entirely consistent with this type of experimental setup. This algorithm was iterated until it converged

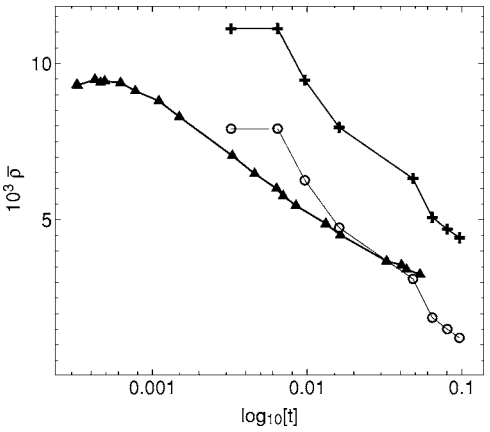

FIG. 2. Comparison of ellipsometry and simulated ellipsometry extracted from best fit x-ray density profiles as a function of t. Ellipsometry (triangles), x-ray profiles (crosses), and x-ray profile with offset of −3.2 (open circles).

on a profile, typically requiring 20 to 100 iterations. The fits are shown as the solid lines in Fig. 1. The uniqueness of the inversion was tested by starting with different initial phase guesses. Both the initial parameter values of Carpenter *et al.* and the best fit values of these parameters to the x-ray data, yield nearly identical real space profiles.

Comparisons were made with the ellipsometry results of Carpenter *et al.* [7], by extracting the optical index of refraction from resulting composition profiles, and simulating the coefficient of ellipticity as defined by $\bar{\rho} = \mathrm{Im}(r_p/r_s)|_{\theta_B}$ as a function of temperature. This procedure is describe in detail elsewhere [7]. This comparison is displayed in Fig. 2.

The x-ray profiles give a reasonable correspondence with the measured temperature dependence of $\bar{\rho}$, however the ellipticity coefficients are offset in the positive direction by 2–4 units. We do not presently understand the basis of this offset. It may be related to differences in the length scale of in-plane surface roughness that is averaged over by each technique. Capillary waves will roughen the interface and the measured interfacial profile will be a convolution of the intrinsic profile and the surface roughness [19]. The surface roughness of the liquid-vapor interface can shift the ellipticity values. The magnitude of the root-mean-square surface height deviations resulting from capillary waves will depend on the area of surface averaged over by the scattering probe, and is typically in the range of 0.3 to 0.7 nm for simple liquids. Since ellipsometry and x-ray measurements may average over different surface areas, they may see different effective interface profiles. The liquid-vapor surface tension remains relatively constant over the range of temperatures measured, so the surface roughness will not show critical scaling and any systematic difference between the ellipsometry and x-ray results would most likely show up as a constant offset. Such an effect may account for part of the shift of the ellipsometry results relative to the x-ray results which we observed. We can estimate an upper bound to this shift by deconvoluting all of the interfacial roughness from our measured experimental profiles. This only shifts the ellipticity factor by around half of the measured difference. Another possible source of the shift could be molecular polarization effects at the surface.

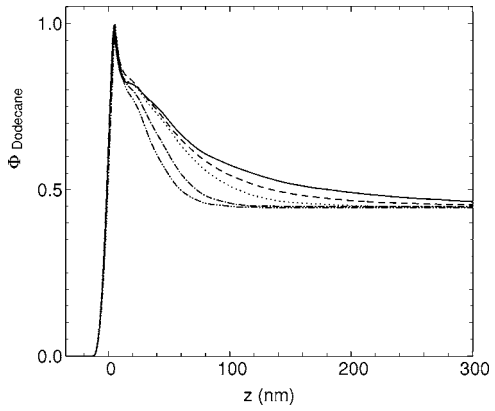

FIG. 3. Volume fraction profiles for dodecane as extracted from the x-ray reflectivity at +1 °C (t=0.0032) (solid line), +3 °C (t =0.0097) (dash line), +5 °C (t=0.016) (dot line), +15 °C (t =0.048) (dot-dash line), and +20 °C (t=0.064) (dot-dot-dash line).

III. SUMMARY OF RESULTS

The extracted volume fraction of dodecane as a function of depth into the fluid are shown vs t in Fig. 3. An unexpected feature of the profiles is an approximately monolayer wide surface layer saturated with dodecane, followed by an abrupt falloff to approximately 83% dodecane. The small rounding of the profile in the region of the monolayer probably results from capillary wave roughness, which cannot be separated from the intrinsic profile.

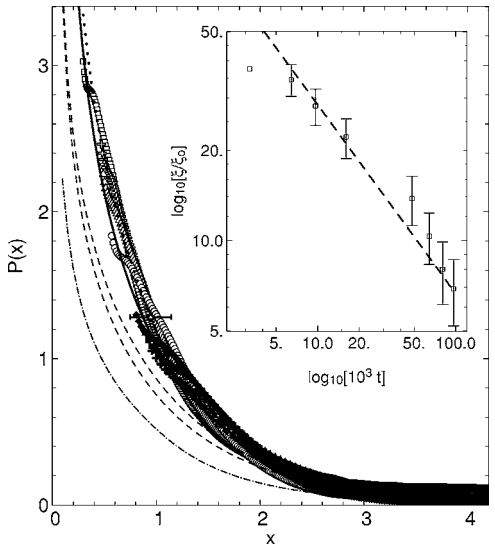

FIG. 4. Comparison of scaled volume fraction data. Experimental data (symbols) with temperatures as in Fig. 1. The dotted line is the best fit to the scaled data using the $P1$ model of Carpenter *et al.* with P_0=1.87, P_∞=1.98, and x_0=0.96. The solid line is the model of Liu and Fisher with the parameters obtained by Jestin *et al.* for the mixture of *n*-hexane+perfluorohexane. The dashed lines are the Liu and Fisher model parameters obtained by Jestin *et al.* for the two methanol+cyclohexane mixtures. The dot-dashed line is the $P1$ model with parameters obtained by Carpenter *et al.* The single error bar is the standard deviation of the fitted values for z_e/ξ along the x axis. The inset shows the best fit value of the scaling ratio ξ/ξ_0. This is shown plotted against the Ising model value of 0.63 (dashed line).

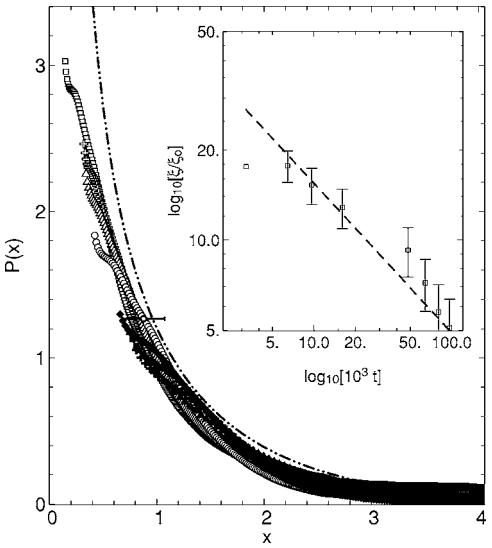

FIG. 5. Comparison of scaled volume fraction data. Experimental data (symbols) with temperatures as in Fig. 1 is compared against mean field theory (dot-dot-dashed line). The inset shows the best fit value of the scaling ratio ξ/ξ_0. This is shown plotted against the mean field model value of 0.50 (dashed line).

The surface composition profile should scale with the bulk correlation length ξ. We have scaled the data sets measured at +2 °C, +3 °C, +5 °C, +15 °C, +20 °C +25 °C and +30 °C to the data taken at +1 °C. This was done in the following manner: the amplitudes of all the volume fraction profiles were divided by t^β according to Eq. (1). The value of β was taken as the Ising value of 0.328. The lowest temperature data set (+1 °C) was then taken as a reference. The volume fraction function for this set was converted to a P function according to Eq. (1) with ξ_0=0.29 nm [7] and z_e =0 for the +1 °C data. The higher T data sets were fit to this set by rescaling them according to $P(x) \equiv P[(z+z_e)/\xi]$ with ξ and z_e adjustable parameters. The first 1 nm of each set was excluded from the scaling since the region near the monolayer should not be expected to scale. The scaled data are plotted in Fig. 4. The scaling gives a reasonable, but not perfect overlap of the data. The error bar on the best fit dotted line represents the standard deviation of the values for z_e/ξ.

In the inset to Fig. 4 the scaling ratio (ξ/ξ_0) obtained from the fits is plotted vs. reduced temperature. Since the scale factor of the +1 °C data was fixed there is no error bar on that point.

In Fig. 4 we have compared the scaled $P(x)$ functions with various predictions. The $P1$ model of Carpenter *et al.* does not match the scaled data using Carpenter's parameters, although excellent agreement can be obtained if one takes P_0=1.87, P_∞=1.98 and x_0=0.96 (dotted line). Very good agreement is also found with the Liu and Fisher model for the parameters found by Jestin *et al.* for *n*-hexane +perfluorohexane.

The scaling represented in Fig. 4 assumes an Ising exponent for β, however it is also of interest to see how well the

data scales using a mean field value of $\beta=0.5$. In Fig. 5 the data were scaled using this value of β and with ξ and z_e adjustable parameters as before. The values of ξ extracted from these fits are shown in the inset to the figure, and compared with the mean field prediction for the exponent $\nu=0.5$. This exponent also provides a reasonable description of the t dependence. The data are compared with the predicted mean field form for $P(x)=\sinh(x)$ [4]. The mean field functional form does not provide as good a fit to the mean field scaled data as the $P1$ model provided for the Ising scaled data. It is, however, still consistent with the experimental uncertainty in the data, chiefly due to the uncertainty introduced by allowing variation in z_e.

The present results differ from previous work in that the composition profiles show a well defined peak corresponding to a monolayer of pure dodecane saturating the surface. There is a subsequent abrupt falloff from this saturated monolayer, to a mixed second layer with $\Phi_{\text{dodecane}}\approx 0.83$. It is not surprising that this monolayer has not been seen before, since no previous probes had comparable spatial resolution. The monolayer thickness, and the magnitude of the discontinuity in composition appears independent of t. This effect will clearly cause scaling to fail within the first nm of the fluid. We cannot exclude the possibility that this monolayer is due to impurities of shorter alkane chains. The larger z portions of the curves do appear to scale, with a form close to an Ising model with $P_0=1.87$, $P_\infty=1.98$, and $x_0=0.96$.

ACKNOWLEDGMENTS

This work was supported by DOE grant DE-FG02-020ER46020. The Advanced Photon Source is supported by DOE grant W-31-109-Eng-38.

[1] M. E. Fisher and P.-G. de Gennes, C. R. Seances Acad. Sci., Ser. B **287**, 207 (1978).
[2] A. J. Liu and M. E. Fisher, Phys. Rev. A **40**, 7202 (1989).
[3] M. Smock, H. W. Diehl, and D. P. Landau, Ber. Bunsenges. Phys. Chem. **98**, 486 (1994).
[4] H. W. Diehl and M. Smock, Phys. Rev. B **47**, 5841 (1993).
[5] G. Floeter and S. Dietrich, J. Phys.: Condens. Matter **97**, 213 (1995).
[6] M. Schlossman, X.-L. Wu, and C. Franck, Phys. Rev. B **31**, 1478 (1985).
[7] J. H. Carpenter, J. H. J. Cho, and B. M. Law, Phys. Rev. E **61**, 532 (2000).
[8] J. H. Carpenter, B. M. Law, and D. S. P. Smith, Phys. Rev. E **59**, 5655 (1999).
[9] J.-H. J. Cho, B. M. Law and K. Gray, J. Chem. Phys. **116**, 3058 (2002).
[10] H. Zhao, A. Penninckx-Sans, L.-T. Lee, D. Beysens, and G. Jannink, Phys. Rev. Lett. **75**, 1977 (1995).
[11] J. R. Howse, J. Bowers, E. Manzanares-Papayanopoulos, I. A. McLure, and R. Steitz, Phys. Rev. E **59**, 5577 (1999).
[12] J. Jestin, L. T. L. M. Privat, and G. Zalczer, Eur. Phys. J. B **24**, 541 (2001).
[13] L. G. Parratt, Phys. Rev. **95**, 359 (1954).
[14] M. Tolan, *X-Ray Scattering from Soft-Matter Thin Films*, Springer Tracts in Modern Physics (Springer, Berlin, 1999).
[15] M. K. Sanyal, S. Hazra, J. K. Basu, and A. Datta, Phys. Rev. B **58**, R4258 (1998).
[16] M. Brown, S. Uran, B. M. Law, L. W. Marschand, L. B. Lurio, I. Kuzmenko, and T. Gog, Rev. Sci. Instrum. **75**, 2536 (2004).
[17] J.-H. J. Cho and B. M. Law, Phys. Rev. Lett. **89**, 146101 (2002).
[18] J. Daillant and A. Gibaud, *X-Ray and Neutron Reflectivity:Principles and Applications*, Lecture Notes in Physics (Springer, Berlin, 1999).
[19] B. R. McClain, M. Yoon, J. D. Litster, and S. G. J. Mochrie, Eur. Phys. J. B **10**, 45 (1999).